THE ASTRONOMICAL JOURNAL, 116:163–179, 1998 July

IONIZATION STRUCTURE IN THE 30 DORADUS NEBULA AS SEEN WITH *HUBBLE SPACE TELESCOPE* WIDE FIELD PLANETARY CAMERA 2

P. A. SCOWEN,[1] J. J. HESTER,[1] R. SANKRIT,[1] J. S. GALLAGHER,[2] G. E. BALLESTER,[3] C. J. BURROWS,[4] J. T. CLARKE,[3] D. CRISP,[5] R. W. EVANS,[5] R. E. GRIFFITHS,[6] J. G. HOESSEL,[2] J. A. HOLTZMAN,[7] J. KRIST,[4] J. R. MOULD,[8] K. R. STAPELFELDT,[5] J. T. TRAUGER,[5] A. M. WATSON,[9] AND J. A. WESTPHAL[10]

Received 1997 December 22; revised 1998 March 20

ABSTRACT

Using the *Hubble Space Telescope* (*HST*) and Wide Field Planetary Camera 2, we have imaged the central 20 pc of the giant H II region 30 Doradus Nebula in three different emission lines. The images allow us to study the nebula with a physical resolution that is within a factor of 2 of that of typical ground-based observations of Galactic H II regions. We present a gallery of interesting objects within the region studied. These include a tube blown by the wind of a high-velocity star and a discrete H II region around an isolated B star. This small isolated H II region appears to be in the midst of the champagne flow phase of its evolution.

Most of the emission within 30 Dor is confined to a thin zone located between the hot interior of the nebula and surrounding dense molecular material. This zone appears to be directly analogous to the photoionized photoevaporative flows that dominate emission from small, nearby H II regions. For example, a column of material protruding from the cavity wall to the south of the main cluster is found to be a direct analog to elephant trunks in M16. Surface brightness profiles across this structure are very similar to surface brightness profiles taken at ground-based resolution across the head of the largest column in M16. The dynamical effects of the photoevaporative flow can be seen as well. An arcuate feature located above this column and a similar feature surrounding a second nearby column are interpreted as shocks in which the photoevaporative flow stagnates against the high-temperature gas that fills the majority of the nebula. The ram pressure in the photoevaporative flow, derived from thermal pressure at the surface of the column, is found to balance with the pressure in the interior of the nebula derived from previous X-ray observations.

By analogy with the comparison of ground-based and *HST* images of M16, we infer that the same sharply stratified structure seen in *HST* images of M16 almost certainly underlies the observed structure in 30 Doradus, which is a crucial case because it allows us to bridge the gap between nearby H II regions and the giant H II regions seen in distant galaxies. The real significance of this result is that it demonstrates that the physical understanding gained from detailed study of photoevaporative interfaces in nearby H II regions can be applied directly to interpretation of giant H II regions. Stated another way, interpretation of observations of giant H II regions must account for the fact that this emission arises not from expansive volumes of ionized gas but instead from highly localized and extremely sharply stratified physical structures.

Key words: H II regions — ISM: individual (30 Doradus) — ISM: structure — Magellanic Clouds

1. INTRODUCTION

30 Doradus is a giant ionized complex in the Large Magellanic Cloud (LMC) located at a distance of 51.3 kpc (see, e.g., Panagia et al. 1991). The nebula is centered on a dense cluster of newly formed stars, the most dense component of which is called R136. The nebula itself is more than 180 pc across, which qualifies it as a smaller member of the elite class of nebulae termed giant extragalactic H II regions. If 30 Doradus was placed at the distance of the Orion Nebula from Earth, it would appear to be more than 20° across and would fill more than 4% of the night sky.

The central cluster is very dense and is composed of several hundred OB stars with a small number of Wolf-Rayet stars (Hunter et al. 1995a). The integrated UV flux from this cluster is intense: more than 50 times that being produced in the center of the Orion Nebula (Campbell et al. 1992). Radiation from the cluster, combined with strong stellar winds from the most massive stars in the cluster, has

[1] Department of Physics and Astronomy, Arizona State University, Box 871504, Tempe, AZ 85287-1504.
[2] Department of Astronomy, University of Wisconsin at Madison, 475 North Charter Street, Madison, WI 53706.
[3] Department of Atmospheric, Oceanic, and Space Sciences, University of Michigan, 2455 Hayward Street, Ann Arbor, MI 48109.
[4] Space Telescope Science Institute, 3700 San Martin Drive, Baltimore, MD 21218.
[5] Jet Propulsion Laboratory, California Institute of Technology, 4800 Oak Grove Drive, Pasadena, CA 91109.
[6] Department of Physics, Carnegie Mellon University, Wean Hall, Pittsburgh, PA 15213-3890.
[7] Department of Astronomy, New Mexico State University, Box 30001/ Department 4500, Las Cruces, NM 88003.
[8] Mount Stromlo and Siding Spring Observatories, Australian National University, Private Bag, Weston Creek, ACT 2611, Australia.
[9] Instituto de Astronomía, Universidad Nacional Autónoma de México, M, J. J. Tablada 1006, Col. Lomas de Santa Maria, 58090 Morelia, Michoacán, Mexico.
[10] Division of Geological and Planetary Sciences, Mail Stop 170-25, California Institute of Technology, Pasadena, CA 91125.

eroded a large cavity in the nearby molecular complex, producing the nebula we see today.

Hunter et al. (1995a) showed that the majority of the stars in the cluster were formed in a single star formation event more than 2–3 million years ago. The census performed yielded a "head count" of more than 3000 stars with more than 300 OB stars capable of producing the intense UV radiation and strong stellar winds responsible for forming and shaping the H II regions we observe in galaxies. The level of star formation exhibited by the 30 Doradus region and the neighboring LMC complex are the closest examples of starburst-like star formation. As such, we are getting a unique view of the star formation environment in the middle of an ongoing starburst.

The average reddening along the line of sight to the LMC and 30 Doradus is very low (Panagia et al. 1991). However, within several H II complexes in the LMC comparison between optical and radio measurements suggests a large variation in the local reddening. Kennicutt & Hodge (1986) found a variation in these estimates between 0 and 1 mag in A_V. Hunter et al. (1995a) also found substantial variation in the reddening across the face of the 30 Doradus Nebula and derived a mean estimate for this reddening of 1.4 mag in A_V at 555 nm and 0.8 mag at 814 nm. For the purposes of this paper we will adopt an extinction of 1 mag in A_V for our observed emission lines.

The 30 Doradus Nebula plays a key role in our understanding of H II regions. Nearby regions are close enough for the physical processes at work within the nebula to be studied in detail. The work by Hester et al. (1996, hereafter H96) on M16, for example, shows that emission within the nebula arises predominantly within a narrow region at the interface between the H II region and the molecular cloud. They follow Hester (1991) in describing this thin region as a photoionized photoevaporative flow. However, an H II region like M16 is tiny in comparison with giant H II regions, and no giant H II regions are close enough to allow the stratified ionization structure of the photoevaporative flow to be studied directly. 30 Doradus alone offers an opportunity to bootstrap the physical understanding of small nearby H II regions into the context of the giant regions seen in distant galaxies.

In this paper, we present *Hubble Space Telescope* (*HST*) images of the ionization structure we observe around the central cluster R136. The wealth of spatial information contained in these pictures is daunting to consider, but we attempt to summarize the most telling points by selecting and presenting several examples of distinct structures around the field of view that provide insight into how the interface with the local gas and dust is evolving. In § 2, we discuss the observations themselves and the general structure of the nebula, as well as presenting full-field mosaics of the data. In § 3, we discuss the conditions apparent in the ionized hydrogen along the walls of the H II region cavity, as well as comparing the ionization structure we observe with models we derive from the Hα surface brightness.

2. OBSERVATIONS AND DATA PROCESSING

Observations of 30 Doradus were obtained on 1994 January 2 using the Wide Field Planetary Camera 2 (WFPC2). Details of the observations are presented in Table 1. Results of the stellar content of R136 derived from the broadband images in this set have been published by Hunter et al. (1995a). Here we present narrowband observations of [O III] λ5007, [S II] λλ(6717 + 6731), and Hα 6563 Å emission from the nebula itself. Images in a relatively line-free continuum band (F547M) were also obtained to distinguish between line emission and stellar reflection luminosity.

The data were processed in the standard way for WFPC2 (Holtzman et al. 1995), including subtraction of dark current offsets, bias frames, and the flat-field correction. Time-dependent hot pixels were subtracted using maps derived from on-orbit dark frames from that general time frame. Cosmic rays were removed using standard anti-coincidence techniques for each pair of images. The images were mosaicked using the appropriate astrometric solution from Holtzman et al. (1995).

Figures 1–4 present the four data sets used in this paper as surface brightness mosaics, Figure 1 being the Hα, Figure 2 the [O III], Figure 3 the [S II], and Figure 4 the F547M. The location of the WFPC2 field is superposed on a *R*-band image from Cerro Tololo Inter-American Observatory of 30 Doradus in Figure 5. Figure 6 presents the full-field color image of the 30 Doradus Nebula. In producing the color image the following steps were taken: (1) all stars were masked off and filled, (2) the [S II] image was included as red, the Hα as green, and the [O III] as blue, and (3) the F170W image was used to replace the hottest stars, also in blue. As presented, the position angle of the field of view for these data is 62° east of north. One WFC pixel represents a linear scale of 7.7×10^{16} cm, or 0.025 pc at the assumed distance of 51.3 kpc to the nebula.

2.1. *General Appearance of the Nebula*

Our field of view is at the very heart of the 30 Doradus Nebula and positions the cluster R136 on the Planetary Camera. As such, our field extends to a radius of 15–20 pc around the center of the nebula, with WF2 to the southeast, WF3 to the southwest, and WF4 to the northwest (cf. Fig. 1). The structure of the nebula is dominated by the ionizing flux from the large number of Wolf-Rayet and early O stars known to be in the cluster (Hunter et al. 1995a). Very close to the center of the cluster there is very little nebulosity, except for a component that can be seen between the cluster stars. This emission could originate either in front of the cluster or behind it, but it does not lie within the interior of the cluster. Intense UV and stellar winds have cleared the cluster itself of dense gas.

Almost all of the nebulosity we observe is concentrated into bright arcs or edges located along the walls of the cavity. Bright rims such as these are commonplace in photoionized nebulae in our own Galaxy. They represent the boundary between the ionized volume and the nearby neutral and molecular gas from which the young cluster was born. The presence of significant X-ray emission within the interior of the nebula and the strongly limb-brightened appearance of these edges suggest that the more diffuse nebulosity arises in such interfaces, but instead seen more face-on.

At a radius of about 5 pc there is a bright circular rim centered on the cluster. This marks the first major interface between the cluster radiation and the nebula's wall. To the west-southwest from R136, this rim is very bright and is littered with finger-like structures that all appear to point toward the cluster. Outside of this rim the brightness of the nebula dims significantly.

One very bright rim is located directly south of the cluster

TABLE 1

DETAILS OF 1994 JANUARY 2 OBSERVATIONS OF 30 DORADUS

Filter	Image Root Numbers	Exposure Time (s)
F336W.....	u25y0101t, u25y0102t	10.0
	u25y0103t, u25y0104t	100.0
F555W.....	u25y0105t, u25y0106t	4.0
	u25y0107t, u25y0108t	40.0
	u25y0109t, u25y010at	200.0
F547M.....	u25y0201t, u25y0202t	5.0
	u25y0203t, u25y0204t	100.0
F814W.....	u25y0205t, u25y0206t	5.0
	u25y0207t, u25y0208t	100.0
F170W.....	u25y0209t, u25y020at	10.0
	u25y020bt, u25y020ct	100.0
F502N	u25y0301t, u25y0302t	500.0
F656N	u25y0303t, u25y0304t	500.0
F673N	u25y0305t, u25y0306t	500.0

and stands out as a bright ridge set against a relatively darker region. As such, we contend that this ridge is directly exposed to the ionizing radiation from the central cluster.

The nature of the photoionized interface at the boundary of a molecular cloud has been discussed in the literature. Heating by UV radiation incident on the interface drives a photoevaporative flow away from the interface (Bertoldi 1989 and references therein). This flow is then photoionized by the same radiation responsible for driving it. Such photoionized photoevaporative flows are characterized by sharply stratified ionization structure (Hester 1991; H96). The overall thickness of the resulting emissive region is typically of order 10^{17} cm, while the observed scale for stratification at the boundary of the cloud can be much less.

By using emission lines arising from species with different ionization states, it is possible to probe the structure of this region. High-ionization lines such as [O III] λ5007 arise in the part of the flow farthest from the interface, where the ionization parameter is high and the radiation field contains enough high-energy photons to reach such ionization states. Emission from species such as [S II] $\lambda\lambda$(6717 + 6731) are brightest beyond the hydrogen ionization edge where the gas density is high and the radiation field is depleted of photons with energies in excess of 13.6 eV. In M16 there is a

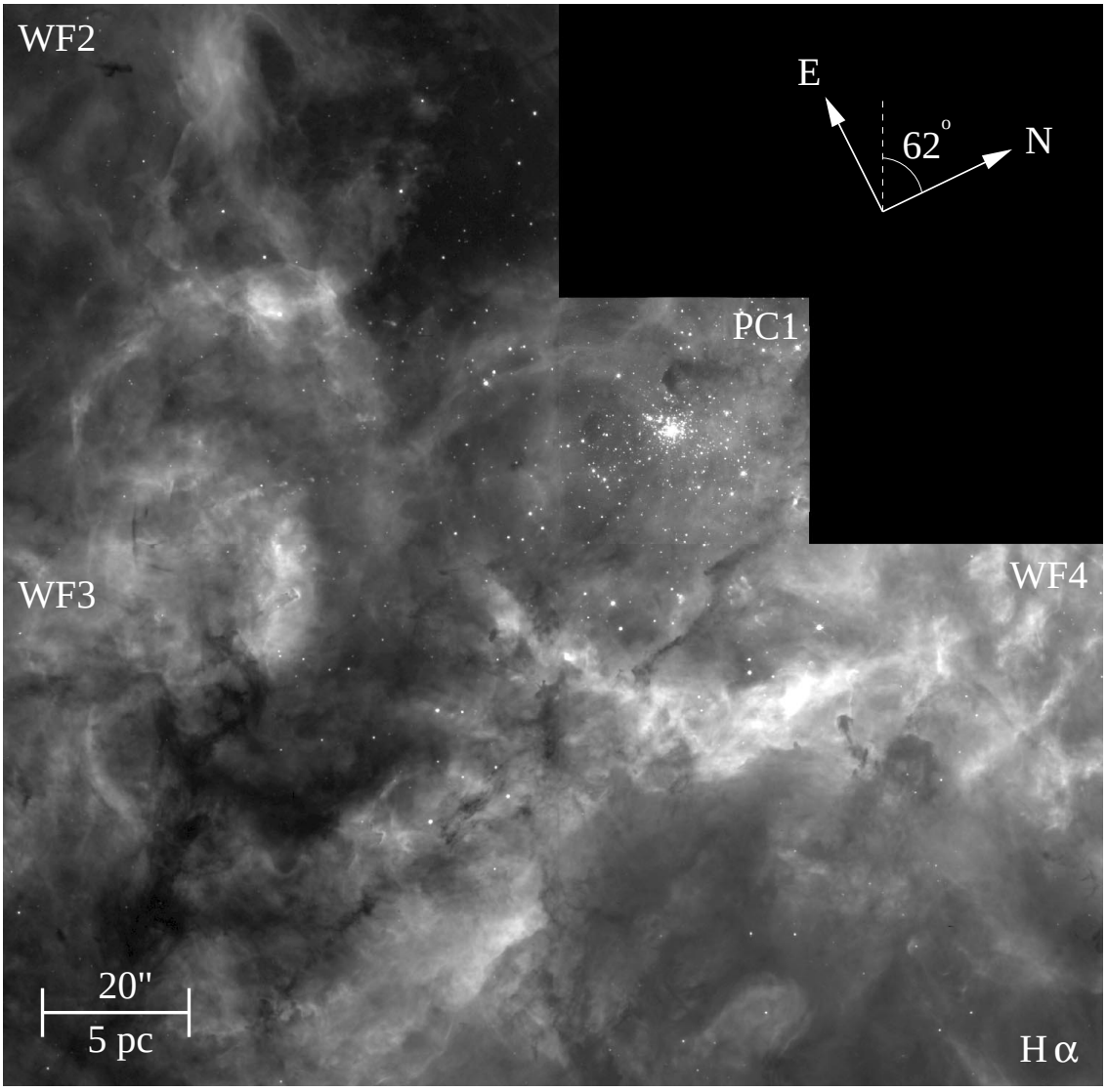

FIG. 1.—Mosaic of the WFPC2 field of the center of 30 Doradus seen in Hα 6563 Å emission. The field orientation is indicated. The core of the cluster and, in particular, the cluster of stars R136 are centered on the PC. The field is characterized by regions of very bright emission from thin interfaces, with a broad diffuse component that covers the face of the nebula. The names of the four WFPC2 chips are included for the unfamiliar reader.

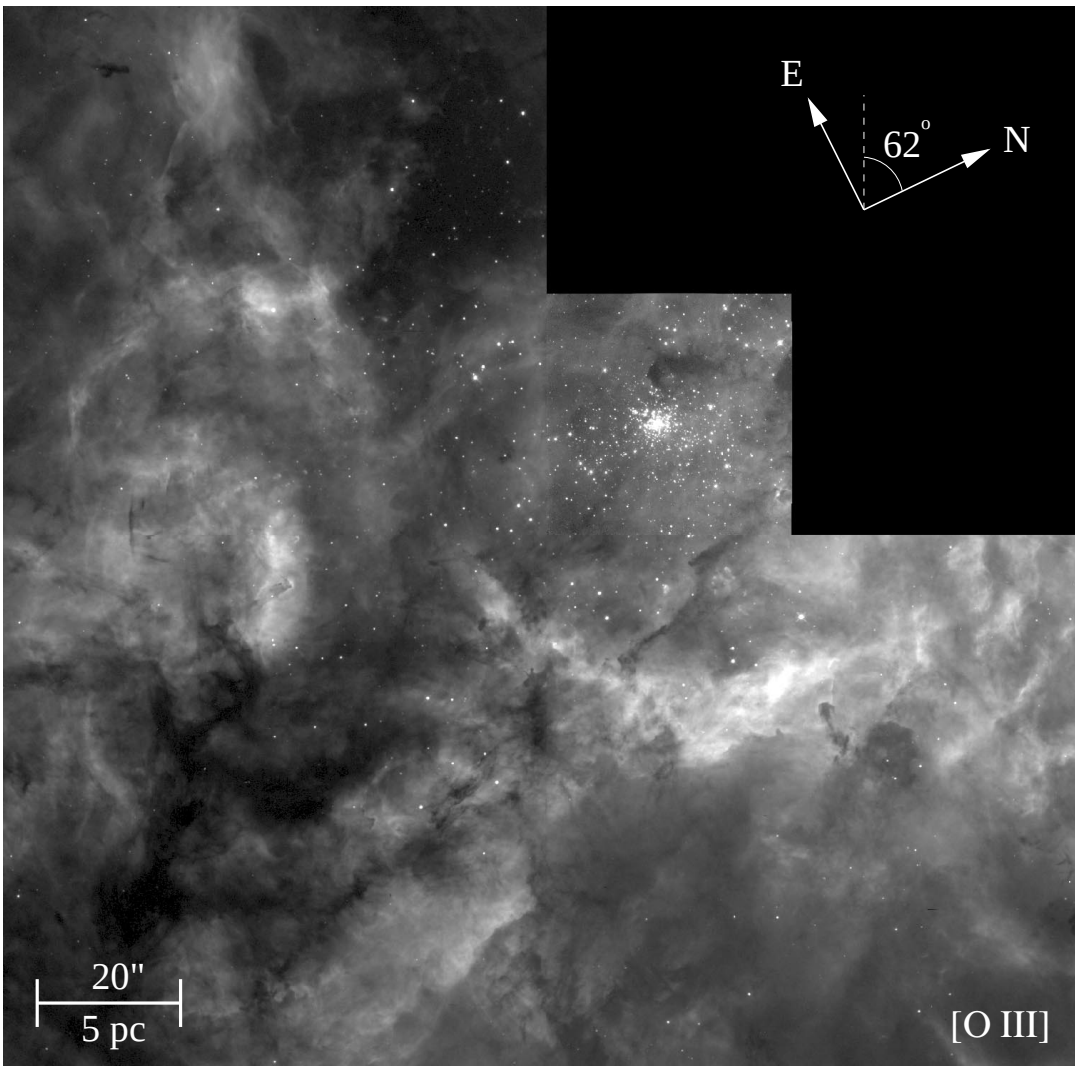

FIG. 2.—Mosaic of the WFPC2 field of the center of 30 Doradus, seen in [O III] λ5007 emission. The field orientation is indicated. The core of the cluster and, in particular, the cluster of stars R136 are centered on the PC. The [O III] emission follows the Hα emission very closely and only departs from it in subtle places.

clear distinction between the peak of the [S II] zone and the peak of the Hα zone, but the two are separated by only 10^{15} cm. H96 found that this structure can be reproduced in detail by photoionization models using a steeply falling density distribution.

Manipulation of photoionization models has revealed that the physical extent of the emission zones and their relative strengths and separations can vary substantially. Factors that can affect these distributions include the steepness of the particle density gradient toward the ionization front, the intensity of the incident ionizing radiation, and the "hardness" of the ionizing radiation (the fraction of photons that fall shortward of the Lyman edge) (H96 and references therein).

While 30 Doradus is too distant to allow resolution of the separation between the Hα and [S II] peaks, it is close enough to see the difference between the highly localized [S II] emission and the thicker zone in which much of the Hα and all of the [O III] originates.

Our images have been taken in the three emission lines mentioned above. Comparing Figures 1–3, we note that while the images differ in several ways, they are also quite similar in many others. In the majority of locations across the nebula the general appearance in the distribution of [O III] emission is almost identical to that of the Hα emission. The nebula looks very different in [S II] $\lambda\lambda$(6717 + 6731) but since these lines are brightest outside of the ionized volume, they trace structure that [O III] and Hα cannot.

Most of the physical structures we observe in 30 Doradus exhibit bright emission in all three of the lines, allowing us to trace a consistent picture of the ionization structure in those locations. Several regions appear bright only in Hα and [S II], indicating that the emission from those regions is characteristic of lower excitation.

In the rest of this section, we are going to visit and describe individual locales in the wall of the nebula. Each will be featured as a morphological prototype for a host of other structures we observed across the field but that we do not have the space to address individually here. The approach we will use employs the three emission lines to compare and contrast the observed physical structure in each line and uses these clues to make some statement about the physical nature of each object.

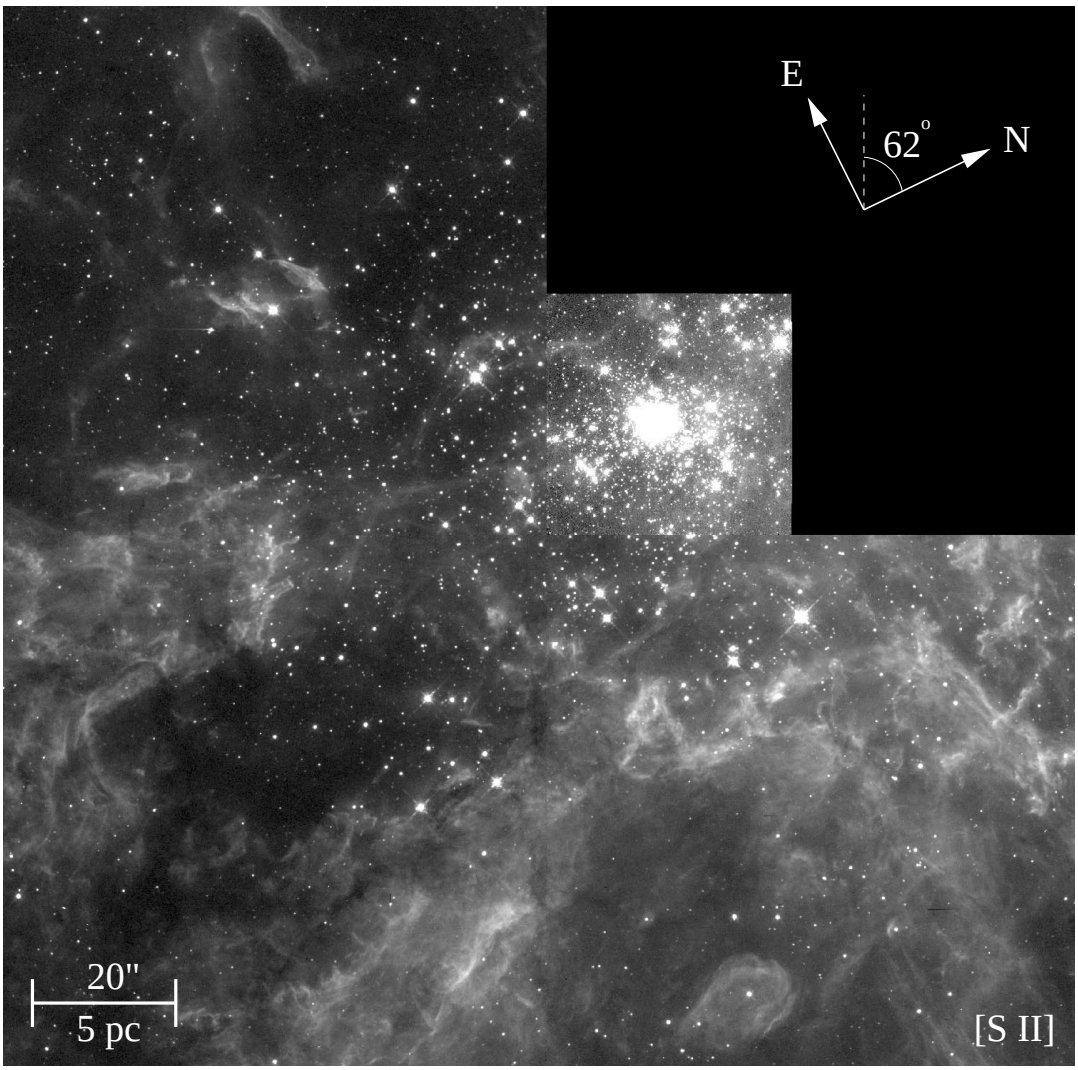

FIG. 3.—Mosaic of the WFPC2 field of the center of 30 Doradus, seen in [S II] $\lambda\lambda(6717 + 6731)$ emission. The field orientation is indicated. The core of the cluster and, in particular, the cluster of stars R136 are centered on the PC. Since the [S II] emission is confined to the regions just exterior to the ionization fronts at the walls of the cavity, only the edges of the nebula show up bright in these lines.

2.2. *Objects of Interest in the Field*

2.2.1. *A High–Proper-Motion Star?*

Toward the top left corner of Figures 1–4 and 6 is a long tubelike structure, especially visible in [S II], which runs approximately east-west. It is rather dim and so has been reproduced in some detail in Figures 7*a*–7*c*. In Figures 7–9 the top panels represent [O III], the middle represent Hα, and the bottom represent [S II].

This object is composed of a long (1.5 pc) limb-brightened tube of emission that is bright in [S II] and is visible in Hα but not [O III]. There is one part of the tube that does show up in [O III] (*top left*), and this corresponds to regions where the Hα and [S II] are brightest. The wall of the tube is also thickest in this region. Elsewhere the wall is almost unresolved, and it appears broken and discontinuous in many locations. The bottom right end of the tube appears to widen to a more spherical shape where a faint star is seen at the heart of the cavity. The very end of the cavity is very fragmented in appearance and has a radius of about 7×10^{17} cm. The center volume of the tube and cavity are relatively dark, contributing little emission. The low-ionization tube lies within a more extended region of diffuse, higher ionization emission. The intensity of the emission from the tube does not depend on distance from the star at its head, indicating that it is ionized externally rather than by the visible star.

The appearance of the system is one of a tube with a relatively dense wall, which provides enough local electron density and column depth to make it brighter in both Hα and [S II] relative to the background nebula. The walls appear to have a resolvable thickness in places, but this appearance might also be produced by limb brightening of an unresolved surface. The apparent "width" of the wall in the top left is about 1.3 WFC pixels, or 10^{17} cm. We infer that the center of the tube is less dense because of the lower emission in that region. The tube is seen to narrow with increasing distance from the star.

We suggest that this structure might be the result of a high–proper-motion star that has a stellar wind. This star appears to be ploughing its way through a cloud of gas of intermediate density. Around the star itself, the wind establishes a balance with the thermal pressure of the local gas and produces the observed cavity. As the star moves

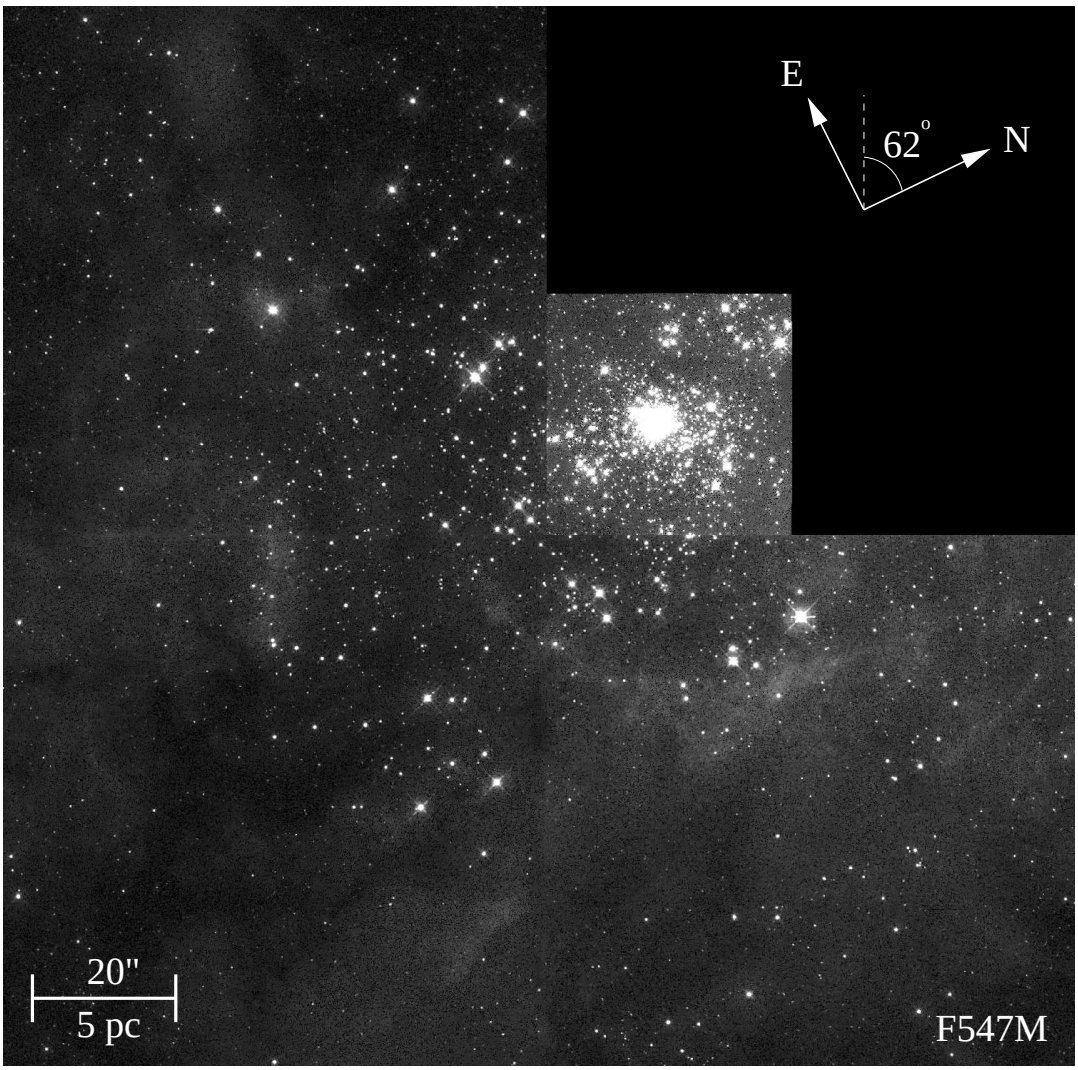

FIG. 4.—Mosaic of the WFPC2 field of the center of 30 Doradus seen in broadband F547M emission. Note the lack of any line emission from the intense nebula. This frame is used to continuum-subtract the line images. The field orientation is indicated. The core of the cluster and, in particular, the cluster of stars R136 are centered on the PC. Many stars are seen in the nebula with some small amount of dust scattering evident in the regions of brightest line emission.

through the cloud, from top left to bottom right in our image, the leading edge of the cavity continues to be pushed into the local gas. On the trailing edge the wall of the cavity persists, to leave a channel or tube through the nebula gas.

If we balance the thermal pressure in the main nebula, obtained from X-ray observations (Wang & Helfand 1991) to be about 10^{-10} ergs cm^{-3}, with the kinetic energy of the material in a wind, then we can infer the density of the material in that wind. The typical velocity of a stellar fast wind is about 10^3 km s^{-1}, which implies a wind particle density of about 10^{-2} cm^{-3}. This corresponds to a mass-loss rate of about $10^{-7}\ M_\odot$ yr^{-1} when integrated across a sphere of radius 7×10^{17} cm. At the point at which the wind's kinetic energy balances the thermal pressure in the nebula, i.e., at the bubble wall, if the gas is at a temperature of 10^4 K, and using the known pressure, we calculate a local particle density of about 50 cm^{-3}.

This is a fairly low density, and one would expect there to be significant [O III] and Hα emission unless that the surrounding material provides enough shielding. This calculation simply balances the momentum in the wind with the thermal pressure of the local nebula gas. If the star does indeed have a significant proper motion, then the mass-loss rate and the gas density in the wall are both lower limits.

This tube will collapse in time as the gas in the tube cools and the surrounding nebula's gas moves to fill the void under thermal pressure. The speed of this collapse would be something like the local sound speed. Using the canonical temperature for photoionized gas of 10^4 K, we estimate the local sound speed to be of order 12 km s^{-1}. We measure the opening half-angle of the tube to be 3°. If all the transverse velocity is produced by the collapse of the tube at the sound speed, the 3° angle implies that the forward proper motion of the star is of order 230 km s^{-1}, which is equivalent to an angular proper motion of 0.95 mas yr^{-1}.

If this is a star with a substantial proper motion, then its path appears to take it directly toward the center of the cluster. If we take the mass of the cluster to be $10^6\ M_\odot$, then at the apparent distance of the tube from the cluster center—about 20 pc—the escape velocity of the cluster is about 20 km s^{-1}. We have calculated an apparent proper motion that is an order of magnitude greater than this.

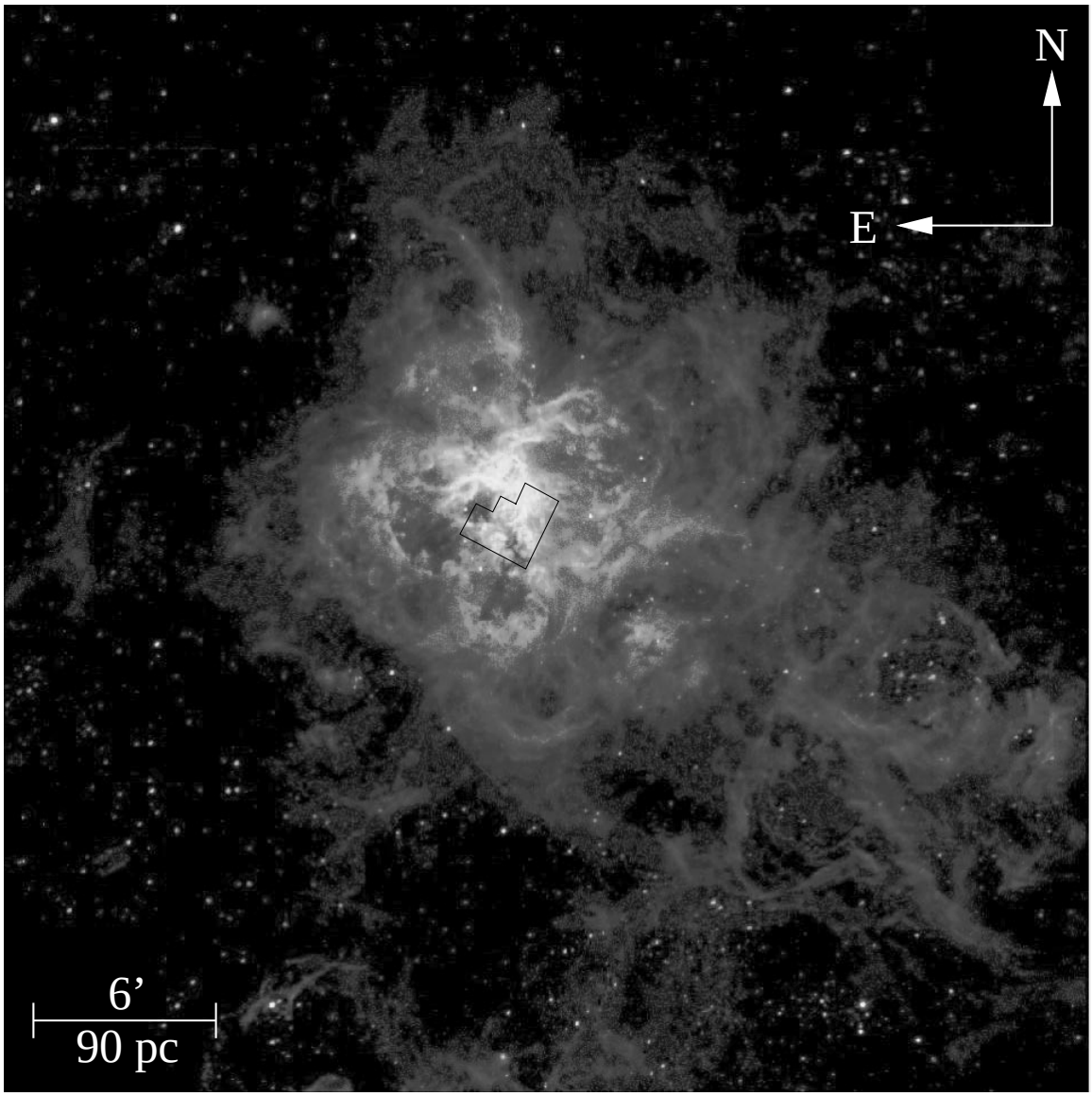

FIG. 5.—CTIO CCD image of the 30 Doradus Nebula. The WFPC2 field of view presented in this paper is indicated at the heart of the object. Note the large size of the overall ionized volume. North is up.

Therefore the star is not bound and is not on a return orbit. The fact that its velocity vector appears to coincide with the cluster is a coincidence.

2.2.2. *Overlapping Bubbles or a Single Cavity?*

Toward the center of WF2 in Figures 1–4 and 6 are a couple of overlapping arcs. These are shown in Figures 7*d*–7*f* and are visible to varying degrees in all three emission lines. The sharpest structure is seen in the [S II] image. Both arcs are covered or masked by appreciable levels of foreground Hα and [O III] emission. The arcs themselves appear quite sharp-edged and appear to brighten toward their edges suggesting that they are probably thin sheets that are limb-brightened, implying that they are seen in projection from one side. At the distance we adopt to the nebula the arcs have a radius of about 1.5 pc with a peak surface brightness of 0.022 ergs cm^{-2} s^{-1} sr^{-1}, or 5.1 $\times$ 10^{-13} ergs cm^{-2} s^{-1} arcsec^{-2}.

Each of the arcs appears to open toward one of the two bright stars seen in the figure. The lower of these two stars has been identified in the ground-based census of stars in the region of the R136 cluster published by Parker (1993) and subsequently included by Walborn & Blades (1997). The other star has not been previously identified but does appear from our data to be redder and therefore later in spectral type than the first star. The lower star is classified as a B0.5 Ia star by Parker (1993), implying the existence of a possible massive wind associated with it. We therefore assume that the lower star is the one responsible for the origin of the arcs, with the upper star being a line-of-sight coincidence with the structures. Recent work by Aufdenberg et al. (1998) has shown that conventional atmosphere models of early B stars have underestimated the hydrogen-ionizing flux they are capable of producing, in some cases by as much as a factor of 2. The helium-ionizing flux may be underestimated by an order of magnitude. As such, it is entirely possible that the lower of these two stars could produce enough flux to ionize the local gas and cause much of the diffuse Hα we see spread across the foreground of this object. The wind from the star might also have been sufficient to sweep up enough material from the region

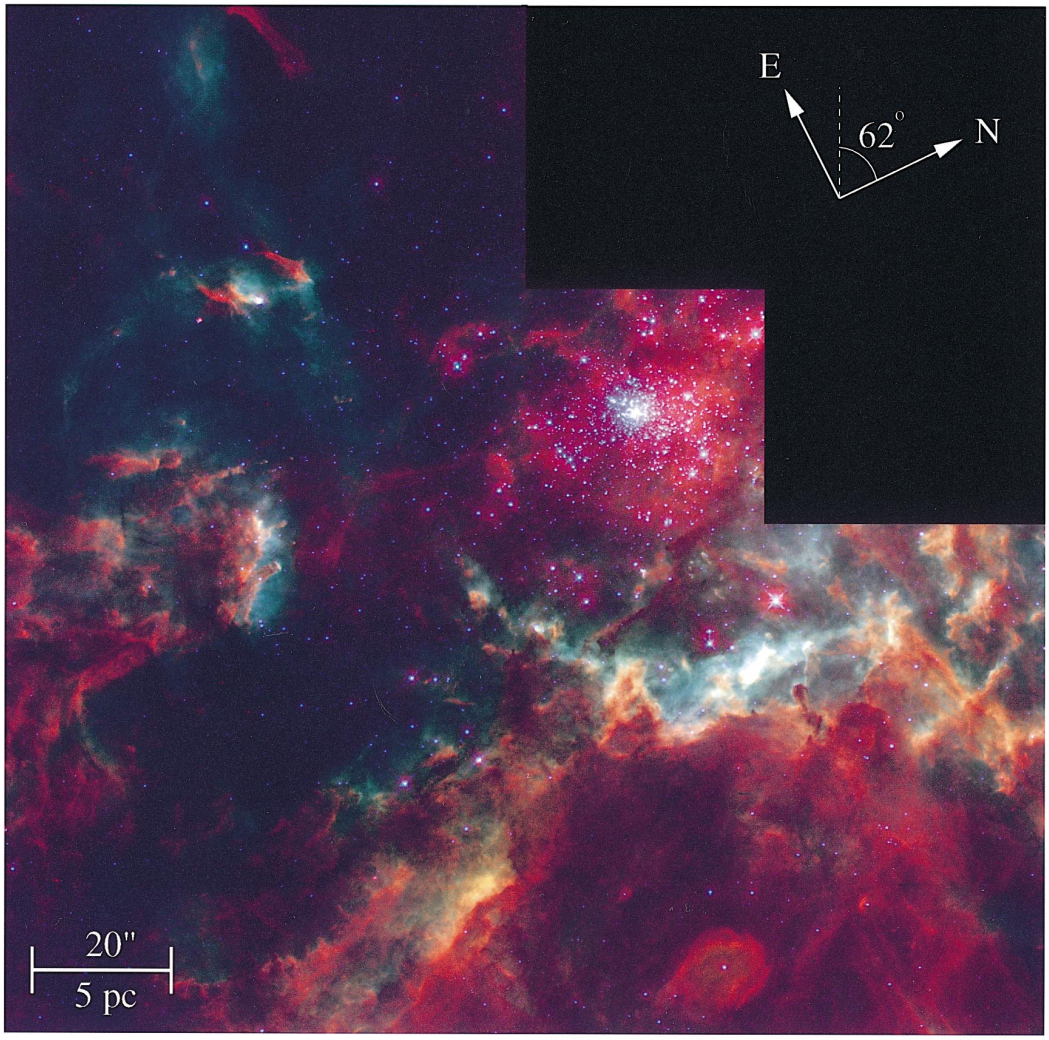

FIG. 6.—Three-color image of the 30 Doradus Nebula. This is a composite of four sets of data: in the nebula's emission blue being [O III] λ5007, green being Hα, and red being [S II] λλ(6717 + 6731); while the stars are replaced with the F170W images as blue. Scale and orientation are indicated.

around the star to produce the thin shell of gas we observe. This shell would then be ionized by the flux from the same star.

2.2.3. *Finger-like Column in the Molecular Wall of the Cavity*

Immediately to the south of the R136 cluster is an isolated region of very bright emission in all three emission lines we observed. Figures 8*a*–8*c* illustrate the structure in the previous manner. Central to the overall morphology of the region are a number of finger-like structures that stick out from the wall of the cavity directly at the main cluster. The main column is about 1 pc long and about 0.25 pc wide. The [O III] and Hα emission are again very similar, while the [S II] is quite different, being concentrated to a narrow region that hugs the wall of cavity. As such, these structures bear a striking resemblance to the columns of dense material observed in M16, the Eagle Nebula, and our own Galaxy and recently studied in great detail with photoionization modeling by H96. The main column we observe in 30 Doradus is directly comparable to the largest column in M16.

Considering the physical scales found to be important in the modeling of the structure observed in M16, we know that these scales are hopelessly unresolved in the 30 Doradus Nebula at a distance some 25 times farther away than M16. Direct comparison between the two nebulae also shows a difference in presentation, with the Doradus finger being viewed more obliquely and through much more foreground emission than M16. Since the visible face of the column is bright in both Hα and [S II], we can state that the near face of the column is directly exposed to the radiation from the cluster. As such we can also state that the column is on the far side of the tangent plane that passes through the cluster and that, therefore, the finger is sticking out of the back wall of the nebula and not a feature of the near wall.

We place the finger on the back wall but not too far into the back, since the foreground emission is not as bright as some regions in the nebula. By doing this we can infer very low levels of intrinsic reddening within the nebula, but we will still adopt our conservative estimate of 1 mag of extinction in A_V.

Based on the similarity in the morphology of the two systems, we explicitly compare M16 to the Doradus finger in § 3 and derive limits on the physical conditions in the nebula despite our much poorer physical resolution at the distance of the LMC. For more details about the structure of this object refer to § 3.

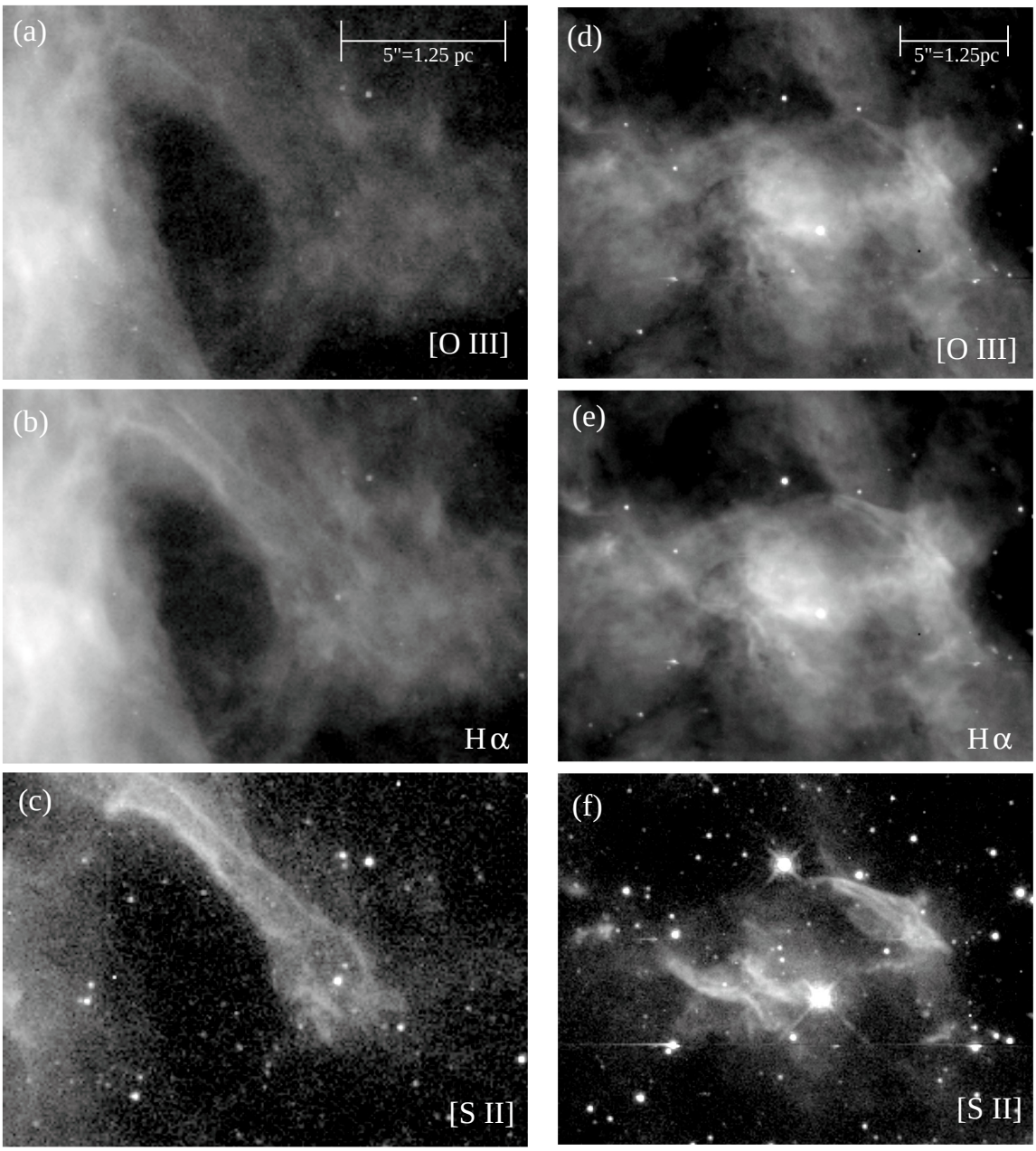

FIG. 7.—*Left*: Tubelike structure found to the southeast of the main cluster, seen in (*a*) [O III], (*b*) Hα, and (*c*) [S II]. *Right*: Double arcs located south-southeast of the main cluster, seen in (*d*) [O III], (*e*) Hα, and (*f*) [S II].

2.2.4. *Low-Excitation* H II *Region*

At the bottom of the field in Figures 1–4 and 6 is a well-defined bubble-like structure about 2–3 pc in diameter. This structure is depicted in the usual way in Figures 8*d*–8*f*. It is characterized by bright emission in both Hα and [S II]. At the geometric center of the region is a bright star not cataloged by any previous survey of the region. Around this star is some very faint diffuse [O III] emission.

These morphological hallmarks, when combined with the absolute levels of the ratio of [S II] to Hα (ranging from less than 0.1 in the center to peaks around 0.3 at the edge) and [O III] to Hα (only ranging between 0 and 0.4 across the bubble), point to a low-excitation H II region centered on the star. This view is supported by the fact that the peak in the lower energy [S II] emission lines occurs exterior to that of the higher line Hα—a known morphological hallmark of a photoionized region. We observe the peak Hα surface brightness to be 0.004 ergs cm^{-2} s^{-1} sr^{-1}, or 9.1×10^{-14} ergs cm^{-2} s^{-1} $arcsec^{-2}$.

The lack of any appreciable [O III] emission in the main body of the small H II region, particularly around the star itself, implies that the ionizing radiation from the star is not very "hard." However, there is still enough flux coming out of the star to ionize an appreciably large volume of gas. This would suggest an early B star as the culprit rather than a late O star. In addition, the bottom left end of the bubble appears open-ended and may represent some type of over-pressure blowout from the cavity into a lower density region. Further observations are needed to clarify the exact physical nature of the system.

An excellent collection of Galactic H II regions, cataloged by Sharpless (1953), were chosen for their strong line emis-

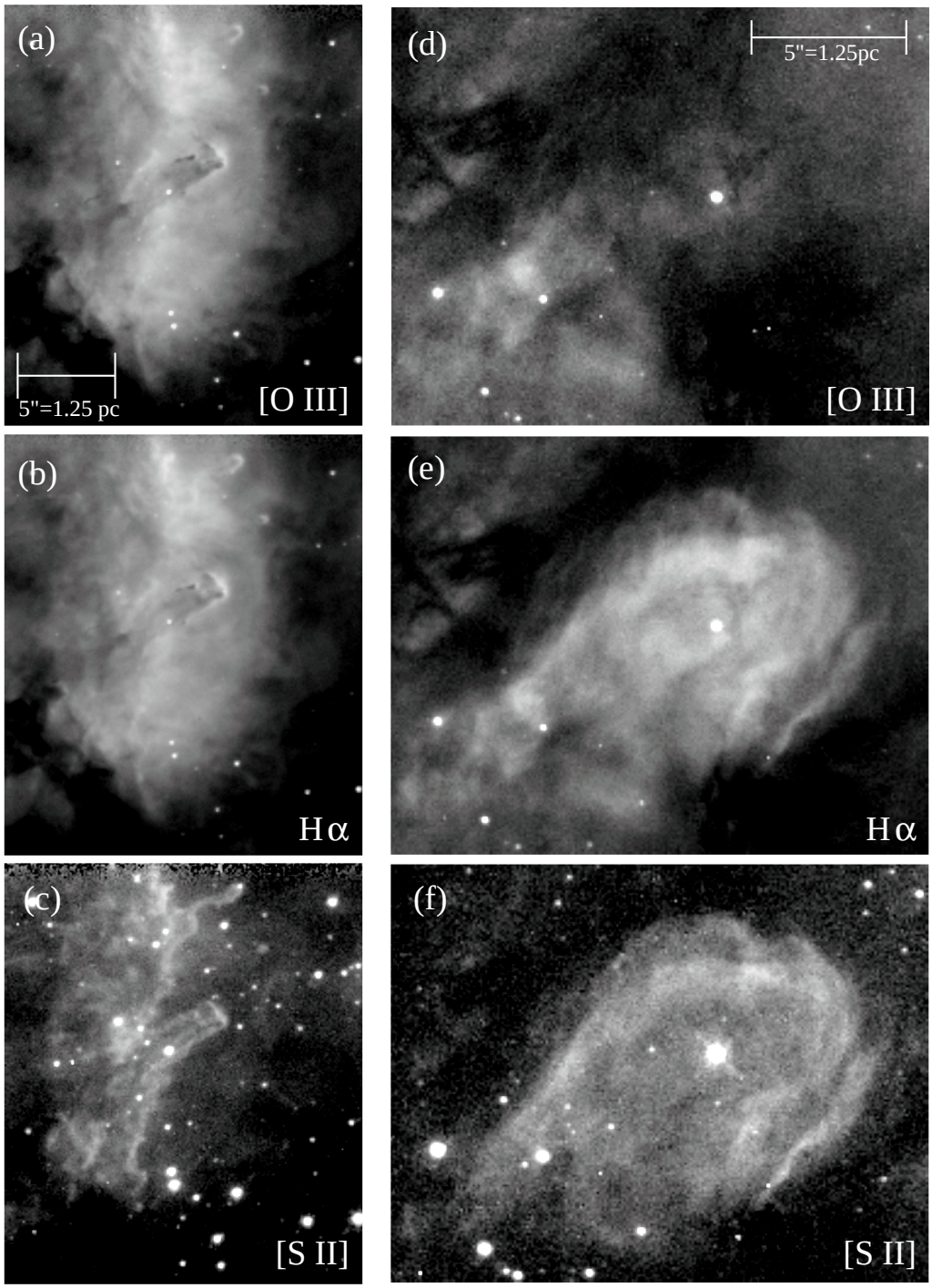

FIG. 8.—*Left*: Finger-like structure found directly south of the main cluster and discussed at length in the text, seen in (*a*) [O III], (*b*) Hα, and (*c*) [S II]. *Right*: Low-excitation H II region located south-southwest of the main cluster that appears to be a foreground object unrelated to the main 30 Doradus cavity, seen in (*d*) [O III], (*e*) Hα, and (*f*) [S II].

sion. Many objects from this sample have been observed by Hester et al. (1992) as part of a morphological atlas of line emission from H II regions. After comparing this bubble-like object with several of the nebulae in this collection, the best analog found was the nebula S104. The observed line ratios and overall shape were very similar. We assume that the two nebulae are also similar in the source and strength of their ionizing sources, allowing us to assume that they are the same physical size based on Strömgren sphere considerations. To equalize the observed diameters of S104 and the bubble nebula, it would have to be placed at a distance of about 50 kpc. This confirms that the bubble nebula is located in the LMC.

It is difficult to place the bubble along the line of sight with respect to the 30 Doradus Nebula. Some of the structure observable in the 30 Doradus Nebula can be seen through the bubble, suggesting that the bubble might be closer to the observer than it is to the main nebula.

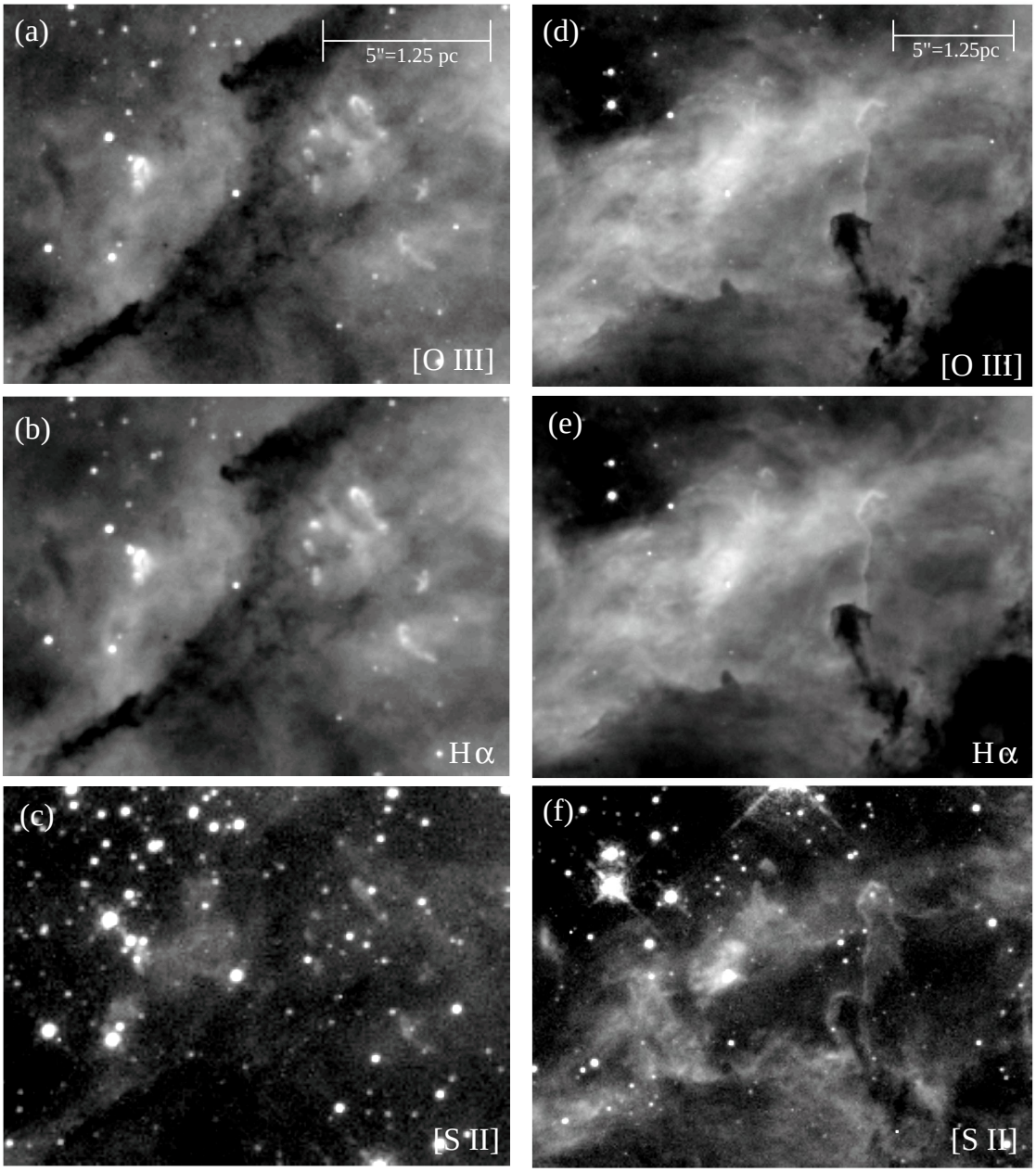

FIG. 9.—*Left*: Smaller blobs of material seen in emission against the bright nebula. These are located close to the cluster and the inner rim of the cavity. Seen in (*a*) [O III], (*b*) Hα, and (*c*) [S II]. Close-up view of main rim in inner cavity. Several outflow-like structures are visible. Seen in (*d*) [O III], (*e*) Hα, and (*f*) [S II].

However, as we stated above, we do know that the bubble nebula is part of the LMC and is therefore more local to 30 Doradus than to our Galaxy.

2.2.5. *Two Views of the Edge of the Main Cavity*

Examination of the images in Figures 1–4 and 6 show a remarkably circular edge to the main cavity—that part of the inner nebula immediately centered on the R136 cluster. This region has a radius of about 8 pc and in our field is characterized by a bright rim to the southwest with numerous large elephant-trunk–like structures. In Figure 9, we present two sets of panels focusing on two particular areas around this bright rim.

Figures 9*a*–9*c* depict a region west-southwest of the cluster with a dark ridge that runs as a chord from rim edge to rim edge. Scattered along the outside of this ridge are several bloblike stuctures with fairly long tails. At this distance our view of these objects is not good, but we can determine some morphological properties. The objects are bright in both Hα and [O III], with the latter appearing marginally sharper around the edge of the objects. In [S II] the objects appear smaller and fainter. These structures are about 2–3 WFC pixels across ($\sim 2 \times 10^{17}$ cm, 13,000 AU, 0.06 pc) and have tails as long as 10–12 pixels [(7–10) $\times$ 10^{17} cm, 65,000 AU, 0.3 pc]. The distribution of emission suggests that the [S II] emission comes from a central core, with the Hα and [O III] emission coming from a bright sheath surrounding the core.

As such, these objects could represent smaller versions of the finger-like column mentioned above. These structures could also be protruding from the cavity wall or could even be separated from the wall. It is not uncommon to find large

globules of this kind floating free in Galactic H II regions (we have found examples in M8 and M17 from the collection of H II regions by Hester et al. 1992), and so it should not be surprising to find analogs in this nebula.

A little further out from the cluster is the main inner cavity edge—seen as a large circular interface around the PC and WFC boundaries in Figures 1–4 and 6. The brightest part of this region is depicted in Figures 9*d*–9*f*. In this field we have two remarkable structures. The lower, darker feature has many common morphological traits with outflows observed in our own Galaxy associated with Herbig-Haro objects and the like. A good physical analog might be HH 47, except that HH 47 is only about 0.6 pc long (Heathcote et al. 1996), whereas the "flows" we observe in 30 Doradus are as long as 1.2 pc. The flow is composed of dense, non–optically emitting gas and appears to broaden into a bow shock–like interface at its end. The narrow end of the structure could be the outflow source and appears to be buried in the cavity wall.

Immediately above this is another structure that appears quite ghostly in Figures 9*d*–9*f*. It is another tall column of material, but its shape and the limb-brightened emission in all three emission lines suggest that it is more like the finger-like structure we considered above. This column measures about 1 pc in length and so is very comparable in size to M16 and the Doradus finger. Buried in the head of this column is a stellar object that may or may not be associated with the column. This object is very close to one of the bright IR sources found in the 30 Doradus Nebula by Hyland et al. (1992) and noted in passing in WF/PC-1 images of the region by Hunter et al. (1995b). The accuracy of the position published by Hyland could place either of these two column-like objects within the positional error bars.

The second column is veiled in very bright foreground emission, making clear definition of the structure hard. When we compare the emission-line profiles across the edge of this structure, we see similar ionization structure characteristics to those found across simple photoionized interfaces. The [O III] and Hα are more extended and appear to be limb-brightened only on the side of the column closest to the central cluster. The [S II] emission is much more concentrated toward the very edge of the column and is spread thinly across the face of the column as well. Because of the bright foreground emission in both [O III] and Hα, we cannot accurately determine how bright the front face of the column really is in these two lines.

Across this particular field we also see many smaller globules and finger-like structures that exhibit similar physical morphology in the three emission lines as do the prototypes we have discussed above. In light of what was learned about photoevaporation in M16 by H96, we expect the majority of the remaining structures in the field to be somewhat denser than their surroundings and perhaps harbor new stars that are in the process of forming.

The remarkable thing about the emission along this cavity edge is the total lack of any emission to the top left (toward the cluster) from this edge. This is apparent too in Figures 1–4 and 6. The volume of the very inner cavity appears totally devoid of any detectable line emission—a direct result of a very low local electron density driving down the emission measure for these lines. The only line emission seen in this region is visible between the stars of the cluster. Estimates for particle densities in the main cavity of 30 Doradus based on diffuse X-ray background emission (Wang & Helfand 1991) suggest number densities around 0.2 cm^{-3}. The same paper also noted several regions or pockets of very hot X-ray–emitting gas associated with "holes" in the optical Hα emission seen from the ground. These regions are probably filled with gas that has been even more strongly shock-excited than the majority of the cavity and may be associated with some of the Wolf-Rayet stars discovered by Hunter et al. (1995a).

3. DISCUSSION

3.1. Hα *Surface Brightness and Photoevaporative Flow*

In § 2.2.3, we described an elephant-trunk structure that is a remarkable analog to the structures in M16. Located about 10^{18} cm from the head of this structure and another nearby elephant trunk are two arcuate emission features. We interpret these features as bow shocks where the diverging photoevaporative flow stagnates against the pressure in the hot gas that fills most of the volume of 30 Doradus (a similar interpretation was offered by H96 for faint filaments in M16). Since the interface at the end of the column in 30 Doradus is concave to the pillar, we assume that the flow is spherically divergent and obeys a $1/r^2$ law for density with distance.

We observe that the surface brightness of this concave bow shock is 3×10^{-4} ergs cm^{-2} s^{-1} sr^{-1} above the bright background, which is equivalent to an emission measure of 1400 cm^{-6} pc. The observed "width" of the bow shock is very thin indeed. It appears to be a limb-brightened shell that has little or no transverse thickness. We put an upper limit on the width of the interface at 2 WFC pixels, or 0.05 pc (1.5×10^{17} cm). If we assume that we are looking at a tangent through a shell of this thickness, then the characteristic line of sight through the wall of that shell will be of order 10^{18} cm. Using the emission measure we observe for the shell wall, this implies a local electron density of about 70 cm^{-3}. This is a lower limit. If this shell is in fact thinner than we can resolve, which is quite likely, then the actual electron density will be higher. If the shell is a factor of 3 thinner (which is the sort of shell thickness observed in Galactic windblown-bubble nebulae such as NGC 7635 and NGC 6888), then the implied electron density is more like 260 cm^{-3}. We observe the radius of curvature of the bow shock to be about 24 pixels, with the end of the column at a radius of about 7 pixels. This implies a factor of 1/12 drop in the flow density from the end of the column to the bow shock, assuming a $1/r^2$ divergence. Therefore the density at the end of the column must be about 3000 cm^{-3}.

The thermal pressure at the end of the column drives the divergence of the gas away from the interface. At the bow shock, the pressure of the photoionized gas is given by

$$P = nkT_e = 2n_e kT_e = 2(260)k \times 10^4 \sim 7 \times 10^{-10} \text{ ergs cm}^{-3} . \quad (1)$$

We need to determine the character of the material in the cavity of 30 Doradus. If it is simply a volume filled with photoionized/photoevaporated material, then the typical electron temperature is something like 10^4 K. However, if the interior gas has been shock-heated by the strong stellar winds from the dozen or so Wolf-Rayet stars found in the cluster (Hunter et al. 1995a), combined with the possible effects of supernovae that have occurred in the cavity since it was formed, then the typical electron temperature is prob-

ably in excess of 10^6 K. Wang & Helfand (1991) presented observations of the diffuse gas in the nebula made with the *Einstein Observatory*. They found a diffuse X-ray component with a characteristic temperature of about 5×10^6 K. From their observations of the X-ray luminosity, they presented a relation between the electron density in the X-ray–bright gas and the overall cavity size. In their paper they assumed that the photoionized gas pressure was more like 1×10^{-10} ergs cm^{-3}, instead of the higher value we calculated by divergence above.

If we balance the divergent ρv^2 flow calculated above with the thermal pressure of an X-ray–bright gas at 5×10^6 K, we predict an electron density of 0.5 cm^{-3} for the hot diffuse gas that fills most of the nebula. This number compares well with the implied estimate by Wang & Helfand of 0.2 cm^{-3}. This is good agreement considering how disparate the two approaches are and the assumptions that have been made.

Next we turn to the emission we see across the top of the column itself. The brightness of the emission at the end of the column allows us to make some statements about the physical conditions in the region in which the emission is most intense. Hunter et al. (1995a) quote an ionizing flux of Lyman continuum photons of 2×10^{51} photons s^{-1} within 93 pc of the cluster center. This number is in good agreement with calculations made by Kennicutt & Hodge (1986) if an internal reddening of 1 mag in A_V is assumed. Here we will adopt this value for the ionizing flux incident on the elephant trunks since at this proximity to the center of the nebula the ionizing flux is dominated by the radiation from R136.

If Q is the ionizing luminosity in units of photons s^{-1} coming out of the cluster, then we can express the incident ionizing flux at the elephant trunks as

$$q = \frac{Q}{4\pi R^2} = \frac{2 \times 10^{51}}{4\pi(5 \times 10^{19}\ \mathrm{cm})^2} = 6 \times 10^{10}$$

$$\text{photons cm}^{-2}\ \text{s}^{-1}\ , \quad (2)$$

where R (=15 pc) is the distance from the ionizing stars. This estimate is made in the plane of the sky and could be much larger if the finger is located on the back wall of the nebula cavity. Assuming that objects such as these are randomly distributed throughout the cavity, we can assess this uncertainty by introducing a factor of $\sqrt{2}$ in our estimate of the distance from the ionizing source. The fraction of these incoming photons that produce a visible Hα photon is given by the ratio of the recombination coefficient for the Hα transition to the total recombination rate for hydrogen as a whole. From Table 4.2 in Osterbrock (1989), we find that the recombination rate for Hα is

$$\alpha_{\mathrm{H}\alpha} = \alpha_{\mathrm{H}\beta} \frac{j_{\mathrm{H}\alpha}}{j_{\mathrm{H}\beta}} \frac{E_{\mathrm{H}\beta}}{E_{\mathrm{H}\alpha}} = 3.03 \times 10^{-14}(2.87)(1.35)$$
$$= 1.17 \times 10^{-13}\ \text{cm}^{-3}\ \text{s}\ , \quad (3)$$

where $E_{\mathrm{H}\alpha}$ is the photon energy for Hα, $E_{\mathrm{H}\beta}$ is the photon energy for Hβ, and all numbers are quoted for conditions of 10^4 K. This predicts that the fraction of Hα photons emerging versus incoming hydrogen-ionizing photons is

$$\frac{\alpha_{\mathrm{H}\alpha}}{\alpha_{\mathrm{B}}} = \frac{1.17 \times 10^{-13}}{2.59 \times 10^{-13}} = 0.453\ . \quad (4)$$

Using equations (2) and (4) we calculate that the expected Hα flux emerging from the end of the column should be 3×10^{10} photons cm^{-2} s^{-1}. If we include the statistical factor of $\sqrt{2}$ for the projection along the line of sight, this could fall as low as 2×10^{10} photons cm^{-2} s^{-1}. This is the emission we expect to be emerging from the end of the column, but we need to factor in the adopted extinction to make an estimate of the expected surface brightness we would measure. Doing this, using 1 mag of A_V, we end up with an estimate of 1×10^{10} photons cm^{-2} s^{-1}.

We need to estimate the size of the emitting region, but we lack one of the dimensions. We can measure the transverse width across the column and the depth of the zone along the radial vector from the cluster, both measured in the plane of the sky. The third dimension, the transverse depth of the emitting zone across the column but perpendicular to the plane of the sky, is unknown. Using our observations we will constrain this depth. If we assess what the emission per unit length across the top of the column is in the plane of the sky, we can use the observed surface brightness to calculate how deep the emission zone must be to produce that level of emission.

The first step is to place an aperture across the top of the column and integrate it across the short dimension of the column. This takes the measured surface brightness in units of ergs cm^{-2} s^{-1} pixel^{-1} and produces an emission per unit length along the top of the column in units of ergs cm^{-2} s^{-1} pixel^{-1}. This is now essentially an integrated profile of the emission across the interface at the end of the column. From this profile we need to choose the value and location that correspond to the thin emission zone at the top of the column, which we know to be unresolved in our data. When we do this we measure a value of 2×10^{-14} ergs cm^{-2} s^{-1} in the one pixel that represents the width of the emission zone at the top of the column. Converting this to Hα photons, we get a flux of 7×10^{-3} Hα photons cm^{-2} s^{-1} in one pixel. This flux needs to be corrected for the 1 mag of extinction we have assumed, increasing the flux estimate to 2×10^{-2} Hα photons cm^{-2} s^{-1} in one pixel.

We next need to take out the effect of the inverse square law by integrating the flux we observe over a sphere of radius 51.3 kpc. This yields a flux of 5×10^{44} Hα photons s^{-1} in that one pixel. The width of that one pixel is 7.7×10^{16} cm at the distance we are assuming for 30 Doradus. Dividing out the physical extent of the pixel along the top of the column we end up with a flux per unit length of 6×10^{27} Hα photons cm^{-1} s^{-1}. Our estimate of the expected Hα flux from the top of the column was 1×10^{10} photons cm^{-2} s^{-1}. If we divide the two quantities we arrive at an estimate for the depth of the emitting region into the plane of the sky. This depth is 6×10^{17} cm, or about 8 WFC pixels. This dimension is very close to the observed transverse width of the column in the plane of the sky, so it is appropriate to think of the column as being cylindrical.

Now that we know the dimensions of the emitting region at the end of the column, we can use the observed surface brightness to make an estimate of the local electron density in the emitting region and compare it with the estimate of 3000 cm^{-3} made independently using the observed bow shock around the end of the column.

The conversion between observed surface brightness and emission measure (EM) is

$$\mathrm{EM} = 2.41 \times 10^3 T^{0.92} S(\mathrm{H}\alpha)\ \text{cm}^{-6}\ \text{pc}\ , \quad (5)$$

where S is the surface brightness expressed in units of ergs $cm^{-2}\ s^{-1}\ sr^{-1}$ (Peimbert, Rayo, & Torres-Peimbert 1975).

We measure the mean surface brightness per pixel to be 1×10^{-13} ergs $cm^{-2}\ s^{-1}$ arcsec^{-2}, or 4×10^{-3} ergs $cm^{-2}\ s^{-1}\ sr^{-1}$. Correcting for an extinction of 1 mag raises these numbers to 2×10^{-13} ergs $cm^{-2}\ s^{-1}$ arcsec^{-2}, or 1×10^{-2} ergs $cm^{-2}\ s^{-1}\ sr^{-1}$. This measurement was made across the brightest region of emission at the top of the column, after having the bright background/foreground subtracted. The corresponding emission measure is 1×10^5 cm^{-6} pc. Using the derived path length through this emission zone of 6×10^{17} cm, or 0.2 pc, we obtain an electron density of about 700 cm^{-3}.

When considering the emission at the end of this column, we have to assess the impact of our lack of sufficient resolution. We have calculated that if we take the observed flux and the observed extent of the emitting region we derive a mean electron density of about 700 cm^{-3}. For M16, H96 shows that the Hα-bright emission zone is of order 2×10^{15} cm, which would be unresolved in our data. Using the data from the *HST* observations of M16, we estimate that the ratio between the observed mean electron density for the region and the value derived from where the emission peaks is about a factor of $\frac{1}{3}$. We also have to assess the difference in path length through the emitting gas. The path length of the line of sight through the region where the emission peaks will be shorter than the path length through the extended emission (since it is farther out from the interface). We estimate this difference in path length to be about a factor of 5 (or a factor of $\sqrt{5}$ in electron density since it is proportional to the square root of path length). Combining these two corrections yields a potential increase in our electron density estimate to about 4700 cm^{-3}. This is an average assessment of the impact of the two effects, and it is entirely possible that slightly different factors should be used in the case of 30 Doradus. Given this uncertainty, this estimate compares well with our earlier independent estimate of 3000 cm^{-3} based on the bow shock. A summary of the numbers we have calculated is included in Table 2, along with numbers calculated for M16 from H96.

In Figure 10, we compare the finger in 30 Doradus with the columns of gas in M16. In addition, we present measured profiles for the three emission lines to illustrate the similarities between the two objects. There are definite differences between the two cases, however, which we will address below.

In conclusion, we have shown that the observed characteristics of the Hα emission at the edge of the 30 Doradus Nebula are well explained by the existence of a photoevaporative flow. We resolve a bow shock transition between the photoevaporative flow and the shock-heated tenuous gas that fills most of the 30 Doradus cavity. The apparent brightness of this interface gives us an independent estimate of the conditions at the head of the column and agrees well with our estimates based purely on the apparent surface brightness coming from the column itself. The column in 30 Doradus is a good morphological analog for the columns observed in M16 by others, but upon closer examination the conditions in 30 Doradus are slightly different.

3.2. *Stratification of the Ionization Structure*

At the distance to the LMC (51.3 kpc), our linear resolution in 30 Doradus is 7.7×10^{16} cm, or about 5000 AU. This compares with the typical resolution achieved by ground-based observations of Galactic H II regions of about 3×10^{16} cm, or about 2000 AU. With *HST* we can study the ionization structure in 30 Doradus in the same way that we have used to studying the structure in local objects.

We cannot, of course, achieve the kind of resolution that was achieved with *HST* imaging of M16 (H96), which allowed successful modeling of the observed structure of the photoionized gas using the known incoming ionizing radiation and the observed density profile of the ionized gas across the edge of the H II region. It is, however, instructive to compare what information we can extract from these data with the picture reached in M16.

The method used to model the structure in M16 started with the observed Hα profile. For a constant path length through the emitting gas, the surface brightness of Hα emission is proportional to the square of the local electron density. This fact allows us to map the local density of neutral gas, which in turn allows a self-consistent photoionization calculation to be made of the observed structure using photoionization codes such as CLOUDY (Ferland 1996). The results achieved in M16 with *HST* were impressive and represented the first time this type of model had been compared directly with observations.

To pursue this approach we need a clean view of an ionization front, and the structure depicted in Figure 10 is again the best choice in our field. We imaged the nebula in three emission lines, each characteristic of a different photoionization energy. The structure of the ionization front in an H II region is predicted by theory to be layered with [O III] emission originating interior to the interface, the Hα emission being concentrated toward the interface and peaking there (by definition), and finally the [S II] is predicted to peak just outside the ionization front (since it has an ionization potential just less than 13.6 eV) with an emitting zone that is very narrow.

When profiles of sufficient resolution are taken across the bright edges of H II regions, these emission line zones form "strata" in which the emission from each line forms a dis-

TABLE 2

COMPARISON OF THE DERIVED PROPERTIES FOR THE PHOTOEVAPORATIVE FLOW FROM THE COLUMN IN 30 DORADUS[a]

Parameter	M16 (*HST*)	30 Doradus
Dimensions of column (pc)	0.3×1.03	0.2×1
Incident ionizing flux (photons $cm^{-2}\ s^{-1}$)	4×10^{11}	6×10^{10}
Total ionizing flux in cluster (photons s^{-1})	2×10^{50}	2×10^{51}
Mean Hα surface brightness (ergs $cm^{-2}\ s^{-1}\ sr^{-1}$)	6×10^{-2}	1×10^{-2}
Depth of low-resolution Hα emission zone (cm)	5×10^{17}	6×10^{17}
Depth of high-resolution Hα emission zone (cm)	6×10^{16}	Unresolved
Mean electron density in Hα-bright zone (cm^{-3})	4000	3000

[a] Compared with published numbers from H96.

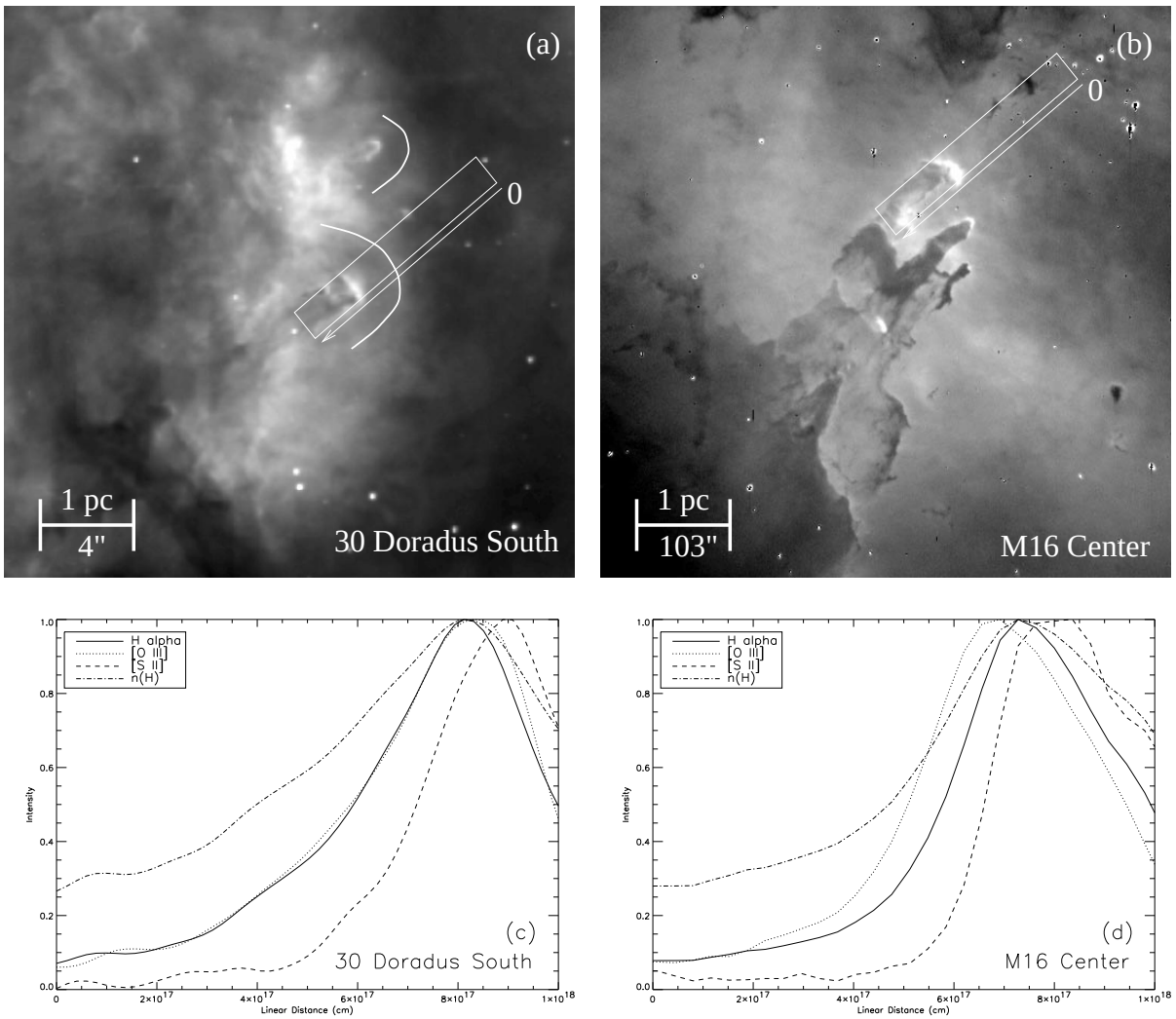

FIG. 10.—(*a*) Picture of the region south of R136 selected to perform ionization structure analysis. The bow shock used in the text is indicated on this picture, along with another one just to the northeast of it. The arrow indicates the direction in which the cut illustrated in (*c*) has been taken. (*b*) The most obvious physical analog to (*a*) is M16 in our Galaxy. This ground-based image of the Eagle Nebula shows the same finger-like morphology and provides a direct comparison for the derived ionization structure from 30 Doradus. Note that the physical scales for (*a*) and (*b*) are the same, but the angular scales are very different. Overlaid are the extracted apertures for each data set. The arrow indicates the direction in which the cut illustrated in (*d*) has been taken. (*c*) Derived emission line profiles for the aperture indicated on (*a*). Note the broad tails on most of the profiles. (*d*) Derived emission-line profiles for the aperture shown on the M16 image.

tinct peak. These peaks are usually separated since the conditions for the emission to be maximized for each line differ in terms of the local electron density and the emissivity of the appropriate species.

In Figure 11*a*, we show the background-subtracted profiles from the column in 30 Doradus plotted as a function of linear distance. The Hα and [O III] peaks are essentially coincident. The [S II] peak is separated from the other two by as much as 10^{17} cm. Employing the density distribution derived from the square root of the Hα profile in Figure 11*a*, we ran a model of the expected photoionization structure at the interface between the H II region cavity and the bounding molecular gas. The other input to this model is the expected hydrogen-ionizing flux from the cluster (calculated above; Hunter et al. 1995a). The appropriate mix of stellar continua was made using the spectral type distribution inferred by the results of Hunter et al. It should be noted that the resulting photon distribution was *harder* than that of the continuum employed for the M16 models in that it had a higher proportion of high-energy photons shortward of the Lyman edge (at 912 Å).

Figure 11*b* depicts the results of this model convolved to the linear resolution of our observations. The *n*(H) plotted is the self-consistent solution from the model, which took as input the profile from Figure 11*a*. At lower radii there are departures from the input profile due to the nature of the fit employed and the boundary conditions placed on the model. In the region where the Hα emission is strong, the resulting *n*(H) closely tracks the observed profile.

Comparison of Figures 11*a* and 11*b* reveals a pretty good match. The Hα and [O III] peaks merge, as we observed, and the narrow [S II] peak becomes more separated from the Hα peak. Thus we have done a reasonable job of reproducing what our observations show as far as the distribution of emission in the three main lines. It is unclear, however, whether this solution is unique.

Figure 11*c* is a reproduction of Figure 10*d*—it depicts the same set of line profiles that we have extracted in 30

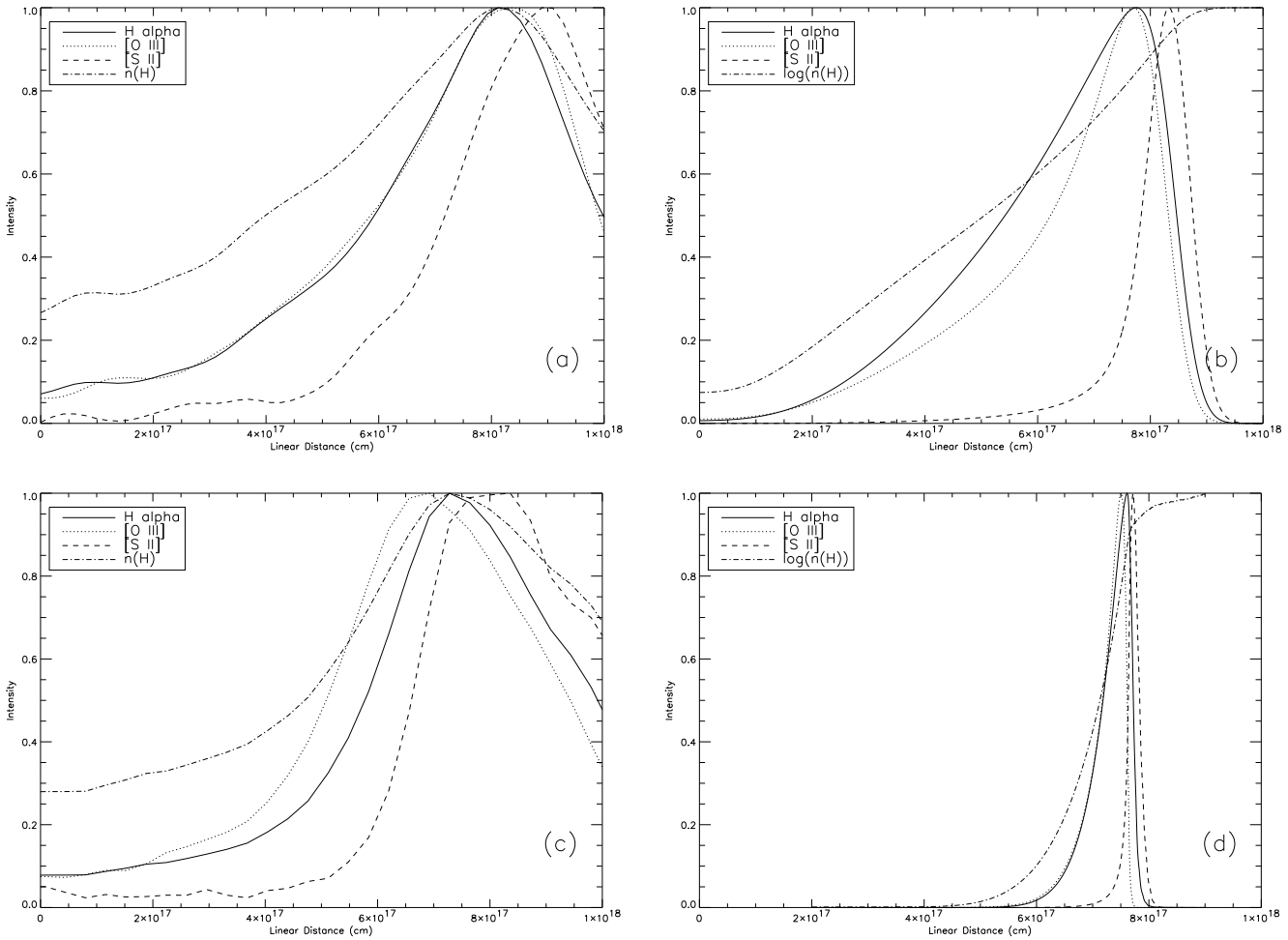

FIG. 11.—(*a*) Extracted emission-line profiles for the aperture shown in Fig. 10 in 30 Doradus. The Hα and [O III] peaks coincide, while the [S II] is markedly separated. The physical scale is indicated in the legend. (*b*) Model of the ionization structure in 30 Doradus using the *n*(H) from (*a*) and convolved to the same linear resolution as (*a*). The peak separations are reproduced, as well as the coincidence of the overall profiles between Hα and [O III]. (*c*) Reproduction of Fig. 10*d* showing the ground-based resolution profiles—note how similar they are in width to those seen in 30 Doradus. (*d*) Model of the structure observed in M16 by H96. This shows how the ground-based data does not represent the true width of the emitting zones. This is also what is happening in 30 Doradus.

Doradus, but this time from ground-based observations of M16, which have been observed at essentially the same linear resolution. Figure 11*d* shows a set of profiles for M16 taken from the best-fit models used in H96, except that this is the model used for column 1 (their paper presented models calculated for column 2). It is included for direct comparison with Figure 11*c*.

What these four graphs show is the remarkable similarity between the structure we observed in 30 Doradus and the structure we observed from the ground in M16. We have matched our observations in 30 Doradus with a model calculated using the same approach as that used by H96. Most of the morphological features are well reproduced—peak separation, approximate zone width, ordering, and so on. However, the critical issue is that while this appears to be a good fit it has been calculated using parameters that we know are incorrect—we know that the actual width of the emitting zones are far narrower than we can resolve. This problem is well illustrated in Figures 11*c* and 11*d*. From the ground we can extract profiles that are very comparable to 30 Doradus and could calculate a similar model in the same way. However, from the model presented in Figure 11*d* we know that the emitting zones for each emission line are very much narrower than we can see from the ground.

Conversely, it does allow us to make an important statement about the structure we observed in 30 Doradus. Throughout this section we have shown in a variety of ways that a picture of a photoevaporative flow is consistent with all the observations we have made. The calculations we have performed by several different methods have yielded the same physical parameters, and together the data support the case for the emission we observe in 30 Doradus to originate in a photoionized photoevaporative flow. By comparing Figure 11*c* with 11*d* and then comparing Figure 11*b* with 11*a*, we can make the statement that the structure we see in 30 Doradus is almost certainly composed of emitting zones far narrower than we can resolve, but that they appear the way we would expect them to given the resolution we can achieve. The structure and emission we observe in 30 Doradus are well explained by exactly the kind of structure observed with *HST* in M16.

There are differences between 30 Doradus and M16, but they are not great. The most significant difference between the two sets of profiles is that in 30 Doradus the Hα and [O III] peaks coincide, whereas in M16 they are well separated. We have already stated that the ionizing flux is more intense in M16, but this should not affect the separation of the Hα and [O III] peaks very much. What is differ-

ent about the two objects is that the ionizing continuum in 30 Doradus is much *harder* than it is in M16 because of the presence of more very massive O stars and a handful of Wolf-Rayet stars. The effect of hardening the ionizing continuum is to compress the [O III] zone toward the ionization front, since more photons of high enough energy will get through to those regions. This would, by inspection of Figure 11, shift the [O III] peak toward the right, making it more coincident with the Hα peak. The picture is still consistent.

4. CONCLUSIONS

We have presented high-resolution narrowband imagery of the 30 Doradus Nebula. There are many interesting localized structures within the nebula, a number of which appear to be associated with winds and UV from stars that are not part of the main 30 Doradus cluster. However, the majority of the emission from the nebula is due to photoionization by the flux from the central cluster. This emission is largely concentrated in thin regions located at the interface between dense molecular material and the shock-heated interior of 30 Doradus.

At the resolution of the *HST* data we find that the structure in 30 Doradus is remarkably similar to what is seen in ground-based observations of nearby H II regions. This similarity is not surprising, given that despite an overall difference in scale, locally the physical conditions in 30 Doradus are not much different than those found in smaller H II regions. We demonstrate this point above by focusing on one particular region in 30 Doradus and showing that it is a very direct analog of the Galactic H II region M16. Taking this same argument a step further, we are led to the conclusion that underlying the observed structure in M16 is the same sort of extremely localized and sharply stratified structure seen in the *HST* images of M16. Thus, even though the 30 Doradus Nebula spans hundreds of parsecs, the emission from this giant H II region arises largely in the same sorts of sharply stratified photoionized photoevaporative flows seen in nearby H II regions.

The 30 Doradus Nebula is a crucial case. The fact that at *HST* resolution 30 Doradus is so similar to ground-based images of nearby H II regions has allowed us to bootstrap our physical understanding based on detailed study of nearby regions into the physical context of a giant H II region surrounding a massive young cluster. Similarly, preliminary analysis of *HST* images of more distant giant H II regions suggests that they compare favorably with 30 Doradus when that nebula is viewed at the same physical resolution. This indicates that conditions in 30 Doradus are probably typical of those found in these distant H II regions as well. Bootstrapping first from nearby H II regions to 30 Doradus in this paper, and, we anticipate, from 30 Doradus to more distant regions in later work, we are approaching the conclusion that the emission from giant H II regions megaparsecs distant is determined by the physics of photoevaporative flows in which relevant physical scales can be as small as 100 AU or less.

The significance of this work lies in the conclusion that the detailed study of nearby, well-resolved H II regions is directly applicable to distant giant H II regions in much the same way that an understanding of radiative shocks that is tested in nearby supernova remnants can be applied in a variety of contexts in which the shock itself is not resolved. Viewed from a different perspective, interpretation of observations of distant giant H II regions must take into account the fact that much of this emission arises not in vast expanses of ionized or even clumpy gas, but instead in well-defined and highly stratified photoevaporative flows localized to the surfaces of molecular clouds.

This work was supported by NASA grant NAS 5-1661 to the WF/PC Investigation Definition Team (IDT) and NASA contract NAS 7-1260 to the WFPC2 IDT. This work was supported at Arizona State University by NASA/JPL contracts 959289 and 959329 and Caltech contract PC 064528.

REFERENCES

Aufdenberg, J. P., Hauschildt, P. H., Shore, S. N., & Baron, E. 1998, ApJ, 498, 837
Bertoldi, F. 1989, ApJ, 346, 735
Campbell, B., et al. 1992, AJ, 104, 1721
Ferland, G. J. 1996, HAZY, a Brief Introduction to Cloudy (Univ. Kentucky Phys. Astron. Dept. Internal Rep.)
Heathcote, S., Morse, J. A., Hartigan, P., Reipurth, B., Schwartz, R. D., Bally, J., & Stone, J. 1996, AJ, 112, 114
Hester, J. J. 1991, PASP, 103, 853
Hester, J. J., Dufour, R. J., Parker, R. A. R., & Scowen, P. A. 1992, BAAS, 23, 1364
Hester, J. J., et al. 1996, AJ, 111, 2349 (H96)
Holtzman, J. A., et al. 1995, PASP, 107, 156
Hyland, A. R., Straw, S., Jones, T. J., & Gatley, I. 1992, MNRAS, 257, 391
Hunter, D. A., Shaya, E. J., Holtzman, J. A., Light, R. M., O'Neil, E. J., & Lynds, R. 1995a, ApJ, 448, 179
Hunter, D. A., Shaya, E. J., Scowen, P. A., Hester, J. J., Groth, E. J., Lynds, R., & O'Neil, E. J., Jr. 1995b, ApJ, 444, 758
Kennicutt, R. C., Jr., & Hodge, P. W. 1986, ApJ, 306, 130
Osterbrock, D. E. 1989, Astrophysics of Gaseous Nebulae and Active Galactic Nuclei (Mill Valley, CA: Univ. Sci.)
Panagia, N., Gilmozzi, R., Machetto, F., Adorf, H.-M., & Kirshner, R. P. 1991, ApJ, 380, L23
Parker, J. W. 1993, AJ, 106, 560
Peimbert, M., Rayo, J. F., & Torres-Peimbert, S. 1975, Rev. Mexicana Astron. Astrofis., 1, 289
Sharpless, S. 1953, ApJ, 118, 362
Walborn, N. R., & Blades, J. C. 1997, ApJS, 112, 457
Wang, Q., & Helfand, D. J. 1991, ApJ, 370, 541